Biosensors and Bioelectronics 126 (2019) 751–757

Contents lists available at ScienceDirect

Biosensors and Bioelectronics

journal homepage: www.elsevier.com/locate/bios

An enzyme-based electrochemical biosensor probe with sensitivity to detect astrocytic versus glioma uptake of glutamate in real time in vitro

Jessica L. Scoggin[a,1], Chao Tan[b,1], Nam H. Nguyen[a], Urna Kansakar[a], Mahboubeh Madadi[c,d], Shabnam Siddiqui[d], Prabhu U. Arumugam[b,d], Mark A. DeCoster[a,b,d], Teresa A. Murray[a,d,*]

[a] Biomedical Engineering, PO Box 10157, Ruston, LA 71272, USA
[b] Institute for Micromanufacturing, PO Box 10137, Ruston, LA 71272, USA
[c] Industrial Engineering, PO Box 10348, Ruston, LA 71212, USA
[d] Center for Biomedical Engineering and Rehabilitation Sciences, Louisiana Tech University, PO Box 10157, Ruston, LA 71272, USA

ARTICLE INFO

Keywords:
Glutamate
Neurochemical probe
Multiple recording sites
Real-time dynamics
Astrocyte
Glioma cell

ABSTRACT

Glutamate, a major excitatory neurotransmitter in the central nervous system, is essential for regulation of thought, movement, memory, and other higher functions controlled by the brain. Dysregulation of glutamate signaling is associated with severe neuropathological conditions, such as epilepsy, and glioma, a form of brain cancer. Glutamate signals are currently detected by several types of neurochemical probes ranging from microdialysis-based to enzyme-based carbon fiber microsensors. However, an important technology gap exists in the ability to measure glutamate dynamics continuously, and in real time, and from multiple locations in the brain, which limits our ability to further understand the involved spatiotemporal mechanisms of underlying neuropathologies. To overcome this limitation, we developed an enzymatic glutamate microbiosensor, in the form of a ceramic-substrate enabled platinum microelectrode array, that continuously, in real time, measures changes in glutamate concentration from multiple recording sites. In addition, the developed microbiosensor is almost four-fold more sensitive to glutamate than enzymatic sensors previously reported in the literature. Further analysis of glutamate dynamics recorded by our microbiosensor in cultured astrocytes (control condition) and glioma cells (pathological condition) clearly distinguished normal versus impaired glutamate uptake, respectively. These results confirm that the developed glutamate microbiosensor array can become a useful tool in monitoring and understanding glutamate signaling and its regulation in normal and pathological conditions. Furthermore, the developed microbiosensor can be used to measure the effects of potential therapeutic drugs to treat a range of neurological diseases.

1. Introduction

Glutamate (Glu), the most prominent excitatory neurotransmitter in the mammalian central nervous system (CNS) (Fonnum, 1984), is tightly controlled throughout the brain and the presence of either too little or too much Glu at synapses is harmful (Zhou and Danbolt, 2014). In the synaptic cleft, excessive Glu concentrations overexcite ionotropic Glu receptors and this leads to neuronal damage and death, known as excitotoxicity (Olney, 1969). Glu is not degraded by enzymatic activity in the synaptic cleft. It is removed from the synapse through diffusion and cellular uptake, such as through excitatory amino acid transporters (EAAT) (Danbolt, 2001), primarily EAAT1 and EAAT2, expressed on astrocytes (Robinson and Jackson, 2016).

Excitotoxicity is associated with seizure activity (During and Spencer, 1993). It has been suggested that impaired Glu uptake contributes both to epileptic seizures (Bryant et al., 2009; During and Spencer, 1993; Tanaka et al., 1997) and to seizures present in glioma patients (Buckingham et al., 2011). EAATs are downregulated in glioma cells (Ye et al., 1999), causing impaired Glu uptake. Additionally, some glioma cells release Glu through the System X_c^- (SXC), a Na^+-independent glutamate/cystine exchanger, further increasing Glu in the surrounding neuronal tissue (Takano et al., 2001; Ye and Sontheimer, 1999). Glioma cells are of interest (Jacobs and De Leo, 2013; Thomas et al., 2015) because glioma cells make up 81% of malignant brain

* Correspondence to: Biomedical Engineering, Louisiana Tech University, PO Box 10157, Ruston, LA 71272-0046, USA.
E-mail addresses: jlk032@latech.edu (J.L. Scoggin), cta019@latech.edu (C. Tan), nhn005@latech.edu (N.H. Nguyen), uka003@latech.edu (U. Kansakar), madadi@latech.edu (M. Madadi), shabnam@latech.edu (S. Siddiqui), parumug@latech.edu (P.U. Arumugam), decoster@latech.edu (M.A. DeCoster), tmurray@latech.edu (T.A. Murray).
[1] These authors shared equally in the work.

https://doi.org/10.1016/j.bios.2018.11.023
Received 19 June 2018; Received in revised form 3 November 2018; Accepted 15 November 2018
Available online 16 November 2018
0956-5663/

tumors and are associated with a high mortality rate (Ostrom et al., 2014). Biosensors that could measure Glu dynamics and distinguish between normal and impaired Glu uptake in real-time could be applied to the evaluation of existing treatments and the development of new treatments for the associated diseases (Robert and Sontheimer, 2014).

Implantable probes have been used to measure extracellular Glu levels (Belay et al., 1999; Mikeladze et al., 2002; Oldenziel et al., 2006; Pomerleau et al., 2003; Tucci et al., 1997). Examples include microdialysis probes, and hydrogel-coated carbon fiber microelectrodes (CFMs) and microelectrode arrays (MEAs). Detection of astrocytic Glu uptake by biochemical assays (e.g., microdialysis for in vivo studies) or colorimetric assays (e.g., for in vitro or ex vivo studies) is highly sensitive but cannot provide high spatial resolution and real-time measures of Glu dynamics. However, measurement of extracellular Glu release and uptake are necessary when studying cellular and circuit mechanisms of neural diseases (McLamore et al., 2010).

In contrast to microdialysis, miniaturized electrochemical microelectrodes using amperometry measurement techniques provide fast, sensitive, and selective real-time recordings of Glu (Ammam and Fransaer, 2010; Salazar et al., 2016; Tian et al., 2009), and improvement to their sensitivity and selectivity has been the major focus of many studies. CFMs have high sensitivity to electroactive neurochemicals (Robinson et al., 2008). However, they have low resistance to biofouling in chronic, in vitro testing and quickly lose their effective surface area and thereby their sensitivity (Dutta et al., 2016). Enzyme-coated platinum (Pt) MEAs offer some advantages over CFMs (Table 1), including multiple recording sites that could lead to better spatial resolution, multiplexing, higher Glu sensitivity (60 vs 320 nA/μM cm^2) (Day et al., 2006; Salazar et al., 2016), and a lower limit of Glu detection (LOD) through its superior sensitivity to hydrogen peroxide (H_2O_2), which is a byproduct of Glu oxidation at the glutamate oxidase (GlOx)-coated biosensor. The LOD range for enzyme-coated Pt microelectrodes is 300–500 nM (Ammam and Fransaer, 2010; Day et al., 2006) while for CFMs, the LOD is 2–5 μM (Oldenziel et al., 2006; Salazar et al., 2016; Schuvailo et al., 2006).

Pt-MEAs can be fabricated with different recording site geometries and with different substrates. Ceramic substrate-based Pt-MEAs are advantageous due to their reduced electrode crosstalk (Burmeister et al., 2000). Ceramic-based Pt-MEAs have been used extensively to measure Glu levels (Day et al., 2006; Hascup et al., 2009; Pomerleau et al., 2003). They are well-characterized (Hascup et al., 2009), have excellent spatiotemporal resolution compared to biochemical assays, can be used to study multiple analytes, and can provide self-referencing sites for interference elimination (Burmeister and Gerhardt, 2001). As such, these MEAs provide an excellent basis for developing and testing new microbiosensor methodology.

Here we have employed a ceramic-based Pt-MEA (CenMeT, KY, USA) to develop an enzyme-based electrochemical MEA microbiosensor probe using the drop casting method. We tested this new probe with respect to its capability to measure in real time and with high sensitivity astrocytic uptake of extracellular Glu in vitro. The probe had a detection range of 10 − 570 μM Glu with 62.3 ± 6.1 nA/μM cm^2 sensitivity in basal media and 270 ± 28 nA/μM cm^2 in phosphate buffered saline (PBS) solution. The latter constitutes an average 3.85-fold improvement in sensitivity over other similarly modified Pt-MEA microbiosensors (Burmeister et al., 2013; Miller et al., 2015). Furthermore, we used the new probe to distinguish between normal Glu uptake in healthy astrocyte cell cultures and impaired uptake in a glioma cell line (CRL-2303 rat glioma).

2. Materials and methods

2.1. Theoretical basis for development of a Glu microbiosensor array

Glu, being non-electroactive, is challenging to detect in real-time. Enzyme-based biosensors of Glu overcome this limitation by selectively oxidizing Glu by the immobilization of GlOx onto the Pt microelectrode, which leads to a secondary electroactive product or reporter molecule, usually H_2O_2. Specifically, GlOx catalyzes Glu into α-ketoglutarate, ammonia, and H_2O_2 (see Eq. (1)).

$$\text{L-glutamate} + O_2 + H_2O \rightleftharpoons \rightleftharpoons 2\text{−oxoglutarate} + NH_3 + H_2O_2 \quad (1)$$

H_2O_2 is then electrochemically oxidized at the Pt microelectrode surface, which is electrically biased at + 0.7 V with respect to a Ag/AgCl reference electrode (Eq. (2)).

$$H_2O_2 \rightarrow O_2 + 2H^+ + 2e^- \quad (2)$$

The magnitude of the generated current is used to measure Glu concentration.

2.2. Fabrication of a Glu microbiosensor array

To create our Glu microbiosensor probes, we used the drop casting method to manually coat commercial Pt-MEA probes (R1, Center for Microelectrode Technology (CenMeT), KY, USA) with GlOx. Platinum was chosen as the electrode material for Glu electrochemical sensing because of its well-known electrochemical properties (Table 1).

R1 probes are ceramic-based MEAs with four 50 μm x 150 μm Pt microelectrode sites, separated by a 50 μm spacing (Fig. 1). The Pt-MEAs were coated with GlOx, as previously described (Miller et al., 2015; Ozel et al., 2014; Weltin et al., 2014; Zhang et al., 2009). Prior to coating, probes were cleaned with 70% isopropyl alcohol and DI water. Then they were blown dry with N_2 and further dried in an oven at 160 °C for 5 min. For enzyme coating, the GlOx enzyme was mixed in de-ionized (DI) water (Continental Water Systems) to prepare aliquots of 0.5 U/μL and stored in − 80 °C upon arrival. Prior to coating, aliquot was transferred to the lab in an ice box and thawed at 4 °C and then at room temperature. DI water (985 μL) was added to 10 mg BSA in a 1 mL centrifuge tube. After allowing the BSA to dissolve, 5 μL of glutaraldehyde (25% in water) was added to the solution. We kept the

Table 1
Platinum and carbon fiber-based microbiosensor performance in the literature.

Electrode	Surface modification	Sensitivity (nA/μM cm^2)	LOD (μM)	Citation
Pt	Pt/mPD/GlOx-silica gel	279	0.005	(Tian et al., 2009)
Pt	Pt/Nafion/GlOx-BSA-GDH	320	0.52	(Day et al., 2006)
Pt	Pt/PPY/MWCNT/GlOx(PU)	384	0.3	(Ammam and Fransaer, 2010)
CF	CF/PB/oPD/PEI/ GlOx-BSA-GDH	135	1.5	(Salazar et al., 2016)
CF	CF-Ru/mPD/ GlOx-BSA-GDH/ Nafion-PU	60	2.5	(Schuvailo et al., 2006)
CF	CF/PEGDGE/GlOx-HRP-AAOx/ Nafion	58	5	(Oldenziel et al., 2006)
Pt	Pt/mPD/GlOx-BSA-GDH	30	0.6	(Burmeister et al., 2013)
Pt	Pt/GlOx-BSA-GDH/mPD	110	–	(Miller et al., 2015)
Pt	Pt/GlOx-BSA-GDH/mPD	270	0.16	This work

Abbreviations. AAOx, ascorbate oxidase; BSA, bovine serum albumin; CF, carbon fiber; GlOx, glutamate oxidase; GDH, glutaraldehyde; HRP, horseradish peroxidase; mPD, m-Phenylenediamine; MWCNT, multiwall carbon nanotube; oPD, o-Phenylenediamine; PEI, polyethyleneimine; PPY, Polypyrrole; PB, Prussian blue; Pt, platinum; PU- polyurethane. PEGDGE, Poly (ethylene glycol) diglycidyl ether; Ru, ruthenium.

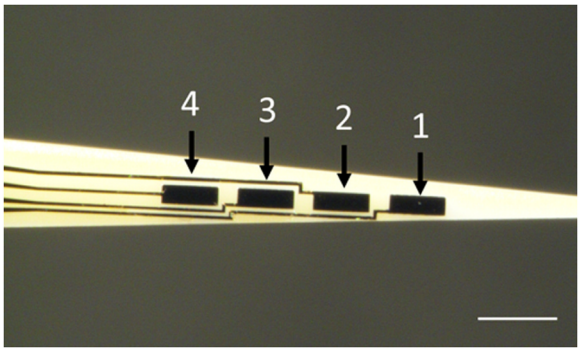

Fig. 1. Uncoated ceramic-based, R1 Pt-MEA (CenMeT, USA) with four recording sites numbered to match reported Glu measurements. Recording sites are 50 × 150 μm with 50 μm between sites. Scale bar denotes 200 μm.

solution mixture (1% BSA and 0.125% glutaraldehyde) at room temperature for 5 mins. A 4 μL volume of the mixture was added to 1 μL of GlOx (0.5 U/μL) and centrifuged to form the final enzyme-matrix mixture of 0.1 U/μL GlOx/0.8% BSA/0.1% glutaraldehyde. A 2 μL micro syringe (Hamilton Co.) was used to manually drop cast the enzyme solution onto the MEA recording sites with the help of a Nikon stereomicroscope (Model, SMZ18). Four drops (~0.05 μL per drop) of the solution was applied in total to each pair of recording sites with a 90 s interval between each drop. The resulting enzyme film thickness was~2.3 ± 0.3 μm (n = 5), which was measured using a Keyence 3D Laser Scanning Confocal Microscope (model VK-X150). Then the probe was stored for 48 h in an aluminum foil covered storage container with no exposure to light prior to coating with a size-exclusion polymer (m-phenylenediamine, mPD) to prevent interferents from reaching the biosensor surface to enhance probe selectivity (Wilson et al., 2017). The mPD layer was electrochemically deposited (cycling between +0.2 V and +0.8 V vs. Ag/AgCl (RE-5B; Bioanalytical Systems, West Lafayette, IN, USA), 50 mV/s, 20 min, 10 mM mPD in 1 M KCl solution). The mPD coating thickness was ~60 ± 9 nm (n = 5).

2.3. Measuring glutamate uptake in astrocytes versus glioma cells

Glu recordings (10 Hz) were acquired in amperometry mode with constant potential (+0.7 V) applied to the developed microelectrodes vs. the Ag/AgCl reference electrode consisting of Teflon coated silver wire (200 μm bare, 280 μm coated; A-M Systems, Carlsberg, WA, USA). A four-channel FAST-16mkIII electrochemical recording system (Quanteon, LLC, Nicholesville, KY, USA) was used to record Glu temporal dynamics.

Prior to each recording session, biosensor probes were first calibrated in PBS buffer using amperometry techniques to evaluate their baseline sensitivity. For amperometry measurements, a multichannel FAST-16mkIII® potentiostat (Quanteon, LLC, Nicholasville, KY) in a 2-electrode configuration was used with an Teflon®-coated Ag/AgCl reference/counter electrode (A-M Systems, Carlsberg, WA, USA). Ag/AgCl reference electrode. A + 0.7 V applied potential was used for H_2O_2 detection. The calibrations were performed in 50 mL PBS solution stirred at 250 rpm and maintained at 37 °C. After a stable baseline was observed, Glu (20 mM) was introduced into the solution using a syringe pump (KD Scientific, Legato® 100 syringe pump) to obtain the desired concentrations of 1, 5, 10, 40, 40 (μM) Glu. Solutions were freshly prepared on the same day that experiments were conducted. All measurements were repeated 6 times (n = 6). Fast analysis® software (Quanteon) was used for data analysis.

Before each in vitro recording session, biosensor probes were calibrated in basal media (see Cell Culture, Section 2.3). To establish a calibration curve, a 35-mm tissue culture treated dish containing 5 mL basal media specific to the cells being tested that day (either astrocytes or CRL-2303 glioma brain tumor cell media) was placed into a custom-made incubator system (Fig. S1, Supplementary Data). The probe was held such that all four probe sites were immersed in the middle of the dish and the microinjector tip for precision dispensing of glutamate was held 12 mm away from the probe and the reference electrode was held 6 mm from the probe. Sturdy probe and injector tip holders were used to consistently place these components at the same positions with respect to the cell culture dish for each experimental session. The biosensor and reference electrodes were immersed into the media and, after a stable baseline current was established, Glu was added in increasing concentrations via micropipette for final media concentrations of 10 μM, 30 μM, 70 μM, and 170 μM. Also, for comparing Glu uptake in astrocytes vs. glioma cells, the same step-wise, increasing concentrations of Glu were added to the same volume of media in experimental dishes with cells.

2.4. Cell culture

Astrocytes derived from primary, newborn Sprague/Dawley rat brain cortices were cultured on 35 mm tissue culture-treated dishes (Falcon®) in Nutrient Mixture F-12 Ham with L-glutamine (0.146 g/L) and sodium bicarbonate (1.176 g/L) from Sigma-Aldrich (St. Louis, MO, USA) with horse serum (5% v/v), fetal bovine serum (5% v/v), and penicillin/streptomycin (0.5% v/v). CRL-2303 (ATCC, C6/lacZ7) rat glioma cells were cultured on Falcon® 35 mm tissue culture-treated petri dishes in DMEM-high glucose (4500 mg/L) from ATCC (Manassas, VA, USA), with L-glutamine (0.584 g/L), sodium bicarbonate (1.5 g/L), and added fetal bovine serum (10% v/v), MEM non-essential amino acid solution 100 × (1% v/v), and penicillin/streptomycin (0.5% v/v). Petri dishes were coated with poly-L-lysine one day prior to plating cells. Both astrocytes and CRL-2303 tumor cells were plated at 750,000 cells per dish. Cells were incubated at 37 °C in a humidified environment with a CO_2 buffer (95% O_2/5% CO_2) and grown to ~80% confluency for experiments. Multiple platings of cells were used on multiple days. Prior to experiments, cells were imaged and then media was replaced with 5 mL fresh, warmed, serum-free basal media (Nutrient Mixture F-12/Ham) with sodium bicarbonate (1.176 g/L, Sigma) and without L-glutamine. After Glu uptake measurement experiments were completed, cells were imaged again. Cellular morphology was used to qualitatively assess the relative health of the cells. While cells sometimes had a slightly narrower morphology at the end of an experiment, they remained adherent and spread on the dish, implying that the cells were alive and functioning. Due to both the length of these experiments (exceeding 5 h per experiment) and the sensitivity of the R1 probe to changes in temperature, dishes of cells were maintained over a home-made water bath placed inside a Heratherm IMC18 bench top incubator (Fig. S1). Bath temperature was maintained between 34.5° to 37.5 °C. The MEAs were also sensitive to electrical noise from lights, motors, and other equipment in the lab. Thus, the incubator door was only opened when necessary.

Carbogen (95% O_2/5% CO_2) was added to the incubator environment for 15 min at the beginning of every experiment to support buffering of the cell culture media. The probe was placed into the center of the dish with all four microelectrodes fully immersed in media (Fig. S1). Glu was added near the outer edge of the 35-mm dish to minimize motion artifact in the recordings. A CMA microdialysis automatic syringe pump was used to drop precise volumes of Glu solution into the media in cell culture dishes.

2.5. Animal care and use

Rat pups were housed with dam. Between days 1 and 3, pups were euthanized by cervical disarticulation according to methods approved by the Louisiana Tech University Institutional Animal Care and Use Committee and in compliance with Directive 86/609/EEC.

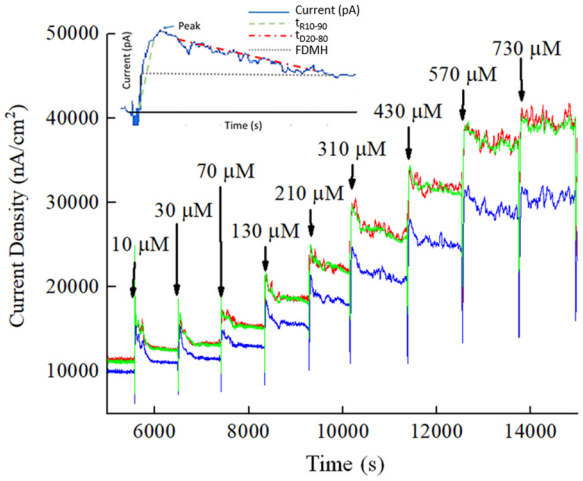

Fig. 2. Current density versus Glu concentration. Response of Glu microbiosensor to stepwise increases in Glu concentration in basal media, as noted on the plot. Sites 2 – 4 are shown (Site 1 malfunctioned; the Site 2 curve overlays Site 4 curve). **Inset.** Depiction of parameters for calculating clearance rate, peak duration and rise time.

2.6. Data analysis

Three parameters, derived from the biosensor's current traces after addition of Glu, were assessed using Origin Pro 2018 software from Origin (OriginLab, Northampton, MA, USA). Specifically, the Quick Peaks Gadget was used to measure peak maxima. The Rise Time Gadget was used to measure rise ($t_{10–90}$) and fall ($t_{20–80}$) times as well as fall velocity (our measure of the clearance rate). The Integrate Gadget was used to assess the full duration at half maximum (FDHM) of the response after Glu addition. These parameters are illustrated in Fig. 2 and defined, as follows: 1) FDHM, also called full width half maximum, is the width of the curve at half the maximum peak. 2) Rise time, $t_{R10–90}$, is the time (s) from 10% to 90% of the trace's rise toward the peak. 3) Fall time, $t_{D20–80}$, is the time (s) from 20% to 80% of the decrease in current from the peak back to a steady trace line. 4) The slope of the line of the fall time $t_{D20–80}$ is the clearance rate, which is also called the fall velocity.

Differences in mean values of the current trace parameters from cultured astrocytes and CRL-2303 cells were compared while accounting for variability in the concentration and blocking for the effect of days on which the experiments were conducted. Multivariate analysis of variance (MANOVA) was used to account for the possible pattern and dependency among the three dependent variables (parameters) in this study and to reduce the probability of Type I error. We also ran a series of analysis of variance (ANOVA) to study the differences in mean probe measurements between the astrocytes and CRL 2303 cells on each response variable. One channel stopped providing signals near the end of the study. This resulted in three instead of four traces for one recording day for astrocytes and two days for glioma cells (n = 44 for astrocytes and n = 40 for glioma cells). To adjust for the missing data, we used the mean imputation method. However, to ensure that data imputation did not significantly distort our data distribution or affect our results, we also ran MANOVA and ANOVA tests using the unbalanced data. The statistical significance threshold α was set to 0.05 for each method, imputed and non-imputed. Although p values were larger without imputation, the statistical significance of differences in mean values for our three measurement parameters did not change. For both methods, the difference in the means were significant for two parameters and not significant for the other parameter. Measurements are expressed as the mean ± the standard error of the mean (SEM).

3. Results and discussion

3.1. Electrochemical characteristics of the developed Glu probe

To determine the electrochemical characteristics of our manually coated and electrodeposited microelectrodes, two tests were performed: (1) tests in basal media to determine the LOD and (2) acute media calibrations to determine biosensor sensitivity. Though the MEA probes from CenMeT are well characterized (Burmeister and Gerhardt, 2001; Pomerleau et al., 2003), possible changes in recording performance due to process variations during the manual and electrodeposition coating, may have occurred. A much higher sensitivity of 270 ± 28 pA/µM cm^2 for in vitro conditions in PBS buffer solution was obtained compared to the published literature (Table S1, Burmeister et al., 2013; Miller et al., 2015). This increase in sensitivity was partly caused by an increased loading of the number of enzymes coated onto the MEA sites. Also, the biosensor demonstrated long-term stability (up to 1 month) with minimal change in Glu sensitivity when stored in DI water at room temperature.

To determine both the LOD and the linear portion of the response to Glu, measurements over a large range of Glu concentrations were acquired using constant-potential (E = +0.7 V with respect to the Ag/AgCl reference electrode) in amperometry mode. A Glu concentration range of 0–730 µM Glu in unstirred basal media was investigated. As seen from the concentration-response data (Fig. 2), the biosensor saturated around 570 µM (37,500 nA/cm^2), beyond which increasing concentrations of Glu no longer resulted in increased current. Current versus concentration was linear for 0 – 570 µM Glu (Fig. S2). The mean sensitivity of the probes in unstirred basal media was 62.3 ± 6.1 nA/µM cm^2 (Table S2). Limit of detection (LOD) is calculated based on "3 × σ/S", where σ is the standard deviation of the baseline (nA/cm^2, 40 data points) and S is sensitivity in nA/µM cm^2 (Burmeister et al., 2001; Ammam et al., 2010; Weltin et al., 2014). The LOD of the biosensor is 6.3 ± 0.95 µM in media and 0.16 ± 0.02 µM in the PBS buffer (n = 5).

Calibration curves for Glu concentration versus current in basal media were produced prior to each in vitro test. The Glu biosensor was positioned over the approximate center of the dish and immersed into basal media, with the fluid covering all four sites (Fig. S1). After a stable baseline was achieved (~1.5–2 h), stock Glu in basal media was added to dishes in 15-min intervals to concentrations of 10 µM, 30 µM, 70 µM, and 170 µM in the dish.

Excellent linearity was observed for all sites (Fig. 3), with coefficients of determination, R^2, of 0.995 or greater. Linear fits for each channel (n = 4) appear in Fig. 3. The linear region of the calibration curve was used to determine the Glu concentration according to Eq. (3):

$$[\text{Glutamate}] = \frac{\Delta\text{Current}}{\text{Slope}} \quad (3)$$

The sensitivity per each recording site was also calculated to investigate possible sensitivity differences across sites of the developed Glu microbiosensor (Table S2, Supplementary Data). Slopes of the calibration tests were averaged across days for the overall sensitivity, which was 62.3 ± 6.1 nA/µM cm^2 (mean ± SEM). As expected, sensitivity differed slightly between probe sites which is likely due to variations in the number of enzymes that are manually applied to each site and to variations in the mPD film thickness and properties during the electrodeposition process. Potential differences in the surface of the Pt microelectrodes may also cause a difference in sensitivity.

3.2. Detection of Glu dynamics in vitro

Comparisons of Glu uptake in cultured astrocytes and the glioma cell line, CRL-2303, were made with special attention to the rise time, full duration at half maximum (FDHM) of the current peak, and the clearance rate (see Fig. 2, inset with parameters) of current traces after additions of

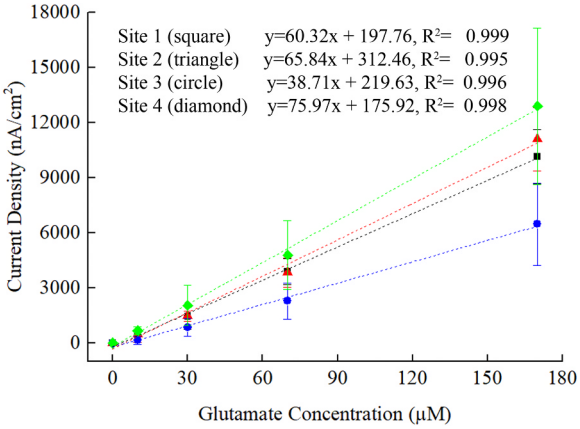

Fig. 3. Basal media calibration using 10, 30, 70, and 170 μM glutamate for each recording site of the biosensor. Current density (nA/cm^2) versus Glu concentration (μM); error bars are SEM. Calibrations in basal media were performed prior to each session to measure glutamate uptake. Dotted and dashed lines denote linear fits for each site. The slopes and linear fits were calculated from measurements taken in basal media (n = 4).

Glu to cell culture media. We used the T_c method, the slope of the most linear portion ($t_{D20–80}$) of the peak decay time, (Daws and Toney, 2007), to compare the clearance rate of Glu in astrocyte and CRL-2303 glioma cell cultures (Fig. 4A, left panel). A statistically significant difference (p = 0.01, imputed; p = 0.02, not imputed) was found between the clearance rate in astrocytes and CRL glioma cells. The T_c (mean ± SEM) for astrocytes was 1.6 ± 0.8 pA s^{-1} (n = 44 tests) while the T_c for the glioma cells was 4.9 ± 1.3 pA s^{-1} (n = 40 tests).

A lower clearance rate, T_c, typically indicates slower clearance. Normally functioning astrocytes are expected to have a faster clearance rate than CRL-2303 tumor cells. This behavior was not what we found in our experiments; however, this may be explained, as follows. According to Vandenberg and Ryan, normal Glu transport has an approximate 50% chance of diffusing away from EAATs on astrocytes only to be bound again before transportation into the cells (Vandenberg and Ryan, 2013). Thus, some of the initially added Glu could be detected by the probe over a more extended period, due to potential release from EAATs. This could contribute to the current at the probe and slow the rate of the return to baseline, producing a slower clearance rate, T_c and extending the peak duration. Residual values (Fig. 4A, right panel) for both cell types are somewhat clustered into levels, suggesting that the clearance rate depends on the concentration of the added Glu. (Residuals are the difference between the value of an individual data point and the mean value.)

Total peak duration times for astrocytes and glioma cells were compared with respect to the full duration at half [peak] maximum (FDHM) for each group (Fig. 4B, left panel). Mean astrocyte responses were significantly longer than the mean tumor cell responses, as mean astrocyte FDHM was 1024 ± 156 s and the mean glioma cell FDHM was 698 ± 133 s (mean ± SEM; p = 0.007, imputed; p = 0.05, not imputed). Furthermore, the deviation from the sample mean detected by the residuals reveals how the peak dynamics in the two groups differed (Fig. 4B, right panel). Residuals for peak duration measurements of astrocytes are grouped in "levels" as we would expect, with larger residual values corresponding to higher levels of Glu concentration. On the other hand, the residuals for glioma cells were tightly grouped around their sample mean, with little difference in duration between concentration levels. This tight grouping indicates a lack of responsiveness by glioma cells to the amount of Glu in solution and hence to increased Glu concentration.

Some glioma cells have been shown to release Glu, even to neurotoxic concentrations, through the SXC exchanger (Ye et al., 1999). However, we did not expect to observe Glu release associated with the SXC exchanger from the CRL 2303 line. This lack of production is supported by prior tests of Glu uptake in these cells using a colorimetric assay (see Supplementary Data). In those tests, no substantial Glu release was detected in comparison to a Glu calibration curve ranging from 50 to 400 μM, similar to our probe calibration range. Impaired uptake is also evident by the lack of levels in the residual values around the rise time mean for glioma cells (Fig. 4B, right panel).

Rise times were also calculated for each group (Fig. 4C, left panel) and found to be 70.3 ± 15.9 s for astrocytes and 52.1 ± 10.6 s for CRL-2303 glioma cells (mean ± SEM). The difference between these mean values was not significant (p = 0.28, imputed; p = 0.35, not imputed). Given that the rise in current at the probe sites was likely dominated by diffusion of added Glu, which was the same condition for both types of cells, the similarity in $T_{R10–90}$ was expected. However, residual values (Fig. 4C, right panel) for astrocyte responses to increasing concentrations of Glu were again grouped in levels corresponding to concentration with no apparent levels for glioma cells. This grouping suggests that Glu uptake by astrocytes in this relatively short time window was dependent upon concentration. We did not simulate Glu diffusion in this work, but this has been done by others, and has been reported to be 0.75 μm^2/ms (Kullmann et al., 1999; Thomas et al., 2011). This diffusion is expected to be increased at physiological temperatures (Thomas et al., 2011), such as was carried out here. Thus, a diffusion of thousands of square microns/second would be expected and it is consistent with rise times in the range of seconds, as we have measured. In this regard, rise time may also be an indicator of time at which concentration equilibration was initially achieved in the dish.

Fig. 5 shows real-time data acquisition for three conditions. These are increasing concentrations of Glu in cell culture media with no cells,

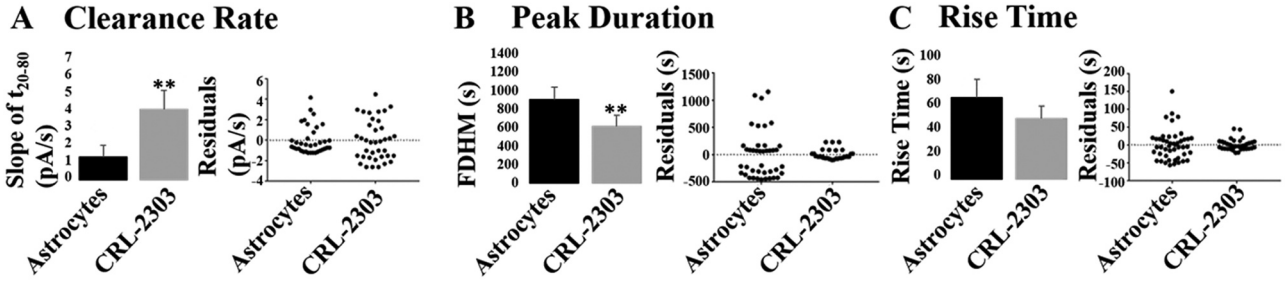

Fig. 4. Significant differences in Glu uptake between astrocytes and glioma cells revealed by features of their respective current traces after additions of increasing concentrations of Glu (10, 30, 70, and 170 μM). **A.** Glu clearance rate. *Left panel:* Clearance rate by astrocytes and CRL-2303 cells. *Right panel:* Scatter plot of residual values. Height difference of residual values in CRL-2303 indicates wider deviation from the sample mean than astrocyte group. **B.** Peak duration (FDHM). *Left panel:* FDHM of the peak current has a longer duration for astrocytes. *Right panel:* Variations in the residuals of after additions of increasingly higher concentrations of Glu are seen clearly as "levels." The more tightly grouped FDHM residuals over all concentrations in glioma cells suggest that these cells are less sensitive to changes in Glu concentration (i.e., impaired). **C.** Rise Time. *Left panel:* Rise times for both cell types were similar. *Right panel:* Residuals exhibit the same distributions as in B. Error bars are mean ± SEM; * * p ≤ 0.01 compared to astrocytes.

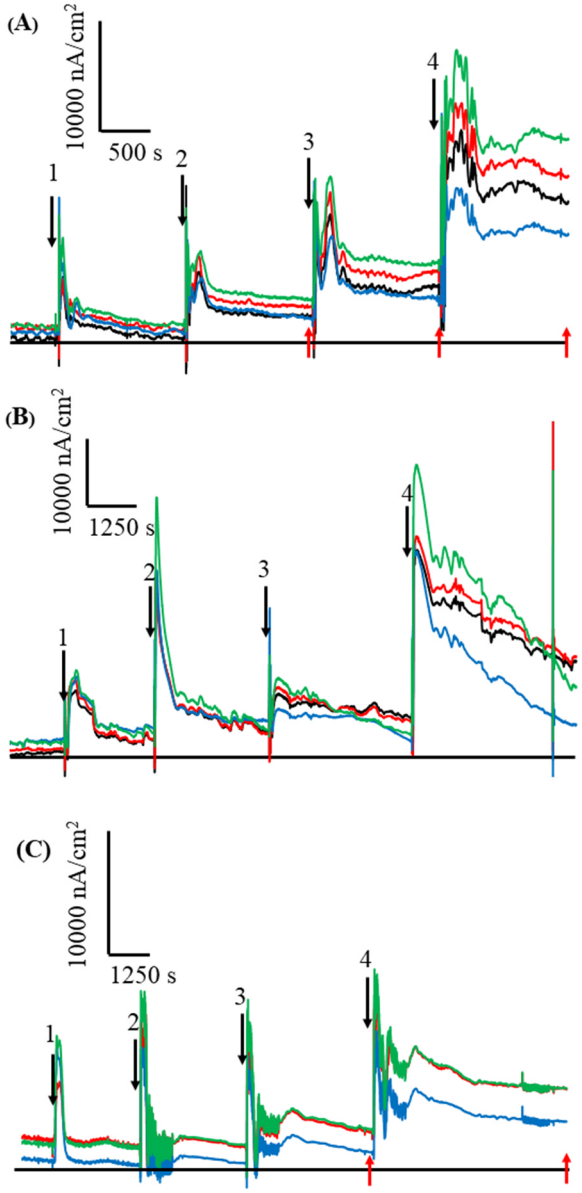

Fig. 5. Representative traces of real-time measurements with increasing Glu concentration. **A.** Basal media without cells shows stepped-like traces as Glu concentration is increased with no return to baseline as Glu concentration is increased (red upward arrows indicate a lack of return to baseline). **B.** Astrocyte traces exhibit a downward trend to the original baseline after each addition of Glu, which indicates Glu uptake. **C.** Glioma cells display stepped-like traces without a return to baseline (red upward arrows) at larger concentrations, similar to the media calibration where no mechanism for Glu uptake exists. Number labels with downward arrows correspond to concentration levels of Glu: 1 = 10 μM, 2 = 30 μM, 3 = 70 μM, 4 = 170 μM. Recording sites are denoted by the colors black (1), red (2), blue (3), and green (4).

with astrocytes, and with glioma cells in the same type of media. During calibration, where no cells are present, and thus no cellular mechanisms for uptake existed, traces appear in an increasing, stepwise manner as Glu was periodically added to the media (Fig. 5A). In contrast, dynamic uptake by astrocytes and diffusion of Glu from transporters, as previously mentioned, contribute to more complex peak dynamics (Fig. 5B). However, traces of current for the CRL-2303 tumor cells (Fig. 5C) were more similar to the recordings in media without cells (Fig. 5A). Thus, the occurrence of stepped-traces in the current recordings can be used as a biomarker for impaired Glu uptake by glioma cells.

As shown in the real-time measurements for astrocytes (Fig. 5B), cells continue to remove Glu from the media in a sustained manner. This removal is apparent in a longer peak duration (Fig. 4B) with a gradual reduction in Glu concentration that continues towards baseline (Fig. 5B), indicating that astrocytes eventually take up all, or most of the added Glu. On the other hand, plots for glioma cells (Fig. 5C) have the same step-like responses as measurements without cells (Fig. 5A) with slower or no return to baseline which is expected for impaired Glu uptake. The transient decreases in current after added Glu reaches a peak concentration in Fig. 5 for no cells (A), astrocytes (B) and glioma cells (C) are due to the consumption of Glu by the biosensor. However, without cells, the signals increase over time as Glu concentration is increased. For impaired glioma cells, a modest return to baseline was observed at low concentrations of glutamate, but at higher concentrations, no return to baseline was observed, suggesting that they were no longer able to take up glutamate.

4. Conclusions

We have developed a highly sensitive, enzyme-based, electrochemical probe that can measure Glu concentration and uptake in real-time and in multiple locations (microarray configuration). The probe can measure 10 – 570 μM Glu in vitro with an overall sensitivity of 62.3 ± 6.1 nA/μM cm^2 in basal media and 270 ± 28 nA/μM cm^2 in PBS buffer, which is a 3.85-fold improvement over other published Pt-MEA Glu biosensors. Further, we have developed a way to analyze the microbiosensor current trace features and distribution of residual values to distinguish between impaired Glu transport in CRL-2303 glioma cells and normal Glu transport in astrocytes. It has been previously suggested that impaired Glu uptake contributes both to the development of epileptic seizures (Bryant et al., 2009; During and Spencer, 1993; Tanaka et al., 1997) and the seizure activity observed in patients with glial tumors (Buckingham et al., 2011). Therefore, the developed probe could be beneficial for monitoring the impairment of Glu transport in diseases ranging from cancer to epilepsy and for evaluating the effects of potential therapeutics to treat these diseases.

Acknowledgements

The authors thank Dr. Leonidas Iasemidis (LI) of Louisiana Tech University as the Principal Investigator on the grant that funded this work and for his useful suggestions on the manuscript. We also thank Dr. Ioannis Vlachos from Louisiana Tech University for assistance with statistical analysis. Additionally, we thank Dr. Steven A. Jones from Louisiana Tech University for his useful suggestions on the manuscript. Funding was provided by a grant from the US National Science Foundation EPSCoR RII-2 FEC OIA1632891 (LI, PA, MAD, and TAM), and a Louisiana Board of Regents Graduate Fellowship (JLS). These funding sources had no role in the design, collection, analysis, or interpretation of data.

Declarations of conflicts of interest

None.

Appendix A. Supporting information

Supplementary data associated with this article can be found in the online version at doi:10.1016/j.bios.2018.11.023.

References

Ammam, M., Fransaer, J., 2010. Biosens. Bioelectron. 25, 1597–1602. https://doi.org/10.1016/J.BIOS.2009.11.020.

Belay, A., Collins, A., Ruzgas, T., Kissinger, P.T., Gorton, L., Csöregi, E., 1999. J. Pharm. Biomed. Anal. 19, 93–105.

Bryant, A.S., Li, B., Beenhakker, M.P., Huguenard, J.R., 2009. J. Neurophysiol. 102, 2880–2888. https://doi.org/10.1152/jn.00476.2009.
Buckingham, S.C., et al., 2011. Nat. Med. 17, 1269–1274. https://doi.org/10.1038/nm.2453.
Burmeister, J.J., Davis, V.A., Quintero, J.E., Pomerleau, F., Huettl, P., Gerhardt, G.A., 2013. ACS Chem. Neurosci. 4, 721–728. https://doi.org/10.1021/cn4000555.
Burmeister, J.J., Gerhardt, G.A., 2001. Anal. Chem. 73, 1037–1042. https://doi.org/10.1021/ac0010429.
Burmeister, J.J., Moxon, K., Gerhardt, G.A., 2000. Anal. Chem. 72, 187–192. https://doi.org/10.1021/ac9907991.
Danbolt, N.C., 2001. Prog. Neurobiol. 65, 1–105. https://doi.org/10.1016/S0301-0082(00)00067-8.
Daws, L.C., Toney, G.M., 2007. CRC Press/Taylor & Francis, pp. 63–82.
Day, B.K., Pomerleau, F., Burmeister, J.J., Huettl, P., Gerhardt, G.A., 2006. J. Neurochem. 96, 1626–1635. https://doi.org/10.1111/j.1471-4159.2006.03673.x.
During, M.J., Spencer, D.D., 1993. Lancet 341, 1607–1610. https://doi.org/10.1016/0140-6736(93)90754-5.
Dutta, G., Tan, C., Siddiqui, S., Arumugam, P.U., 2016. Mater. Res. Express 3, 094001. https://doi.org/10.1088/2053-1591/3/9/094001.
Fonnum, F., 1984. GJ. Neurochem. 42, 1–11.
Hascup, E.R., et al., 2009. Brain Res. 1291, 12–20. https://doi.org/10.1016/j.brainres.2009.06.084.
Jacobs, V.L., De Leo, J.A., 2013. J. Neurooncol. 114, 33–42. https://doi.org/10.1007/s11060-013-1158-7.
Kullmann, D.M., Min, M.Y., Asztely, F., Rusakov, D.A., 1999. Philos. Trans. R. Soc. Lond. B 354, 395–402.
McLamore, E.S., et al., 2010. J. Neurosci. Methods 189, 14–22. https://doi.org/10.1016/j.jneumeth.2010.03.001.
Mikeladze, et al., 2002. Electroanalysis 14, 393–399. https://doi.org/10.1002/1521-4109(200203)14:6<393::AID-ELAN393>3.0.CO;2-P.
Miller, E.M., Quintero, J.E., Pomerleau, F., 2015. J. Neurosci. Methods 252, 75–79. https://doi.org/10.1016/J.JNEUMETH.2015.01.018.
Oldenziel, W.H., Dijkstra, G., Cremers, T.I.F.H., Westerink, B.H., 2006. Brain Res. 1118, 34–42. https://doi.org/10.1016/J.BRAINRES.2006.08.015.
Olney, J.W., 1969. Science 164, 719–721. https://doi.org/10.2307/1726016.
Ostrom, Q.T., et al., 2014. Neuro. Oncol. 16, 896–913. https://doi.org/10.1093/neuonc/nou087.
Ozel, R.E., Ispas, C., Ganesana, M., Leiter, J.C., Andreescu, S., 2014. 52, 397–402. ⟨https://doi.org/10.1002/nbm.3066.Non-invasive⟩.
Pomerleau, F., Day, B.K., Huettl, P., Burmeister, J.J., Gerhardt, G.A., 2003. Ann. N. Y. Acad. Sci. 1003, 454–457.
Robert, S.M., Sontheimer, H., 2014. Cell Mol. Life Sci. 71, 1839–1854. https://doi.org/10.1002/nbm.3066.non-invasive.
Robinson, D.L., Hermans, A., Seipel, A.T., Wightman, R.M., 2008. Chem. Rev. 108, 2554–2584.
Robinson, M.B., Jackson, J.G., 2016. Neurochem. Int. 98, 56–71. https://doi.org/10.1016/j.neuint.2016.03.014.
Salazar, P., Martín, M., O'Neill, R.D., González-Mora, J.L., 2016. Sens. Actuators B Chem. 235, 117–125. https://doi.org/10.1016/J.SNB.2016.05.057.
Schuvailo, O.M., Soldatkin, O.O., Lefebvre, A., Cespuglio, R., Soldatkin, A.P., 2006. Anal. Chim. Acta 573–574, 110–116. https://doi.org/10.1016/J.ACA.2006.03.034.
Takano, T., Lin, J.H., Arcuino, G., Gao, Q., Yang, J., Nedergaard, M., 2001. Nat. Med. 7, 1010–1015. https://doi.org/10.1038/nm0901-1010.
Tanaka, K., et al., 1997. Science 276, 1699–1702. https://doi.org/10.1126/science.276.5319.1699.
Thomas, A.G., et al., 2015. PLoS One 10, e0127785. https://doi.org/10.1371/journal.pone.0127785.
Thomas, C.G., Tian, H., Diamond, J.S., 2011. J. Neurosci. 31 (12), 4743–4754. https://doi.org/10.1523/JNEUROSCI.5953-10.2011.
Tian, F., Gourine, A.V., Huckstepp, R.T.R., Dale, N., 2009. Anal. Chim. Acta 645, 86–91. https://doi.org/10.1016/J.ACA.2009.04.048.
Tucci, S., Rada, P., Sepúlveda, M.J., Hernandez, L., 1997. J. Chromatogr. B. Biomed. Sci. Appl. 694, 343–349.
Vandenberg, R.J., Ryan, R.M., 2013. Physiol. Rev. 93, 1621–1657. https://doi.org/10.1152/physrev.00007.2013.
Weltin, A., Kjenjinger, J., Enderle, B., 2014. Biosens. Bioelectron. 61, 192–199. https://doi.org/10.1016/J.BIOS.2014.05.014.
Wilson, L.R., Panda, S., Schmidt, A.C., Sombers, L.A., 2017. Anal. Chem. 90, 888–895.
Ye, Z., Sontheimer, H., 1999. Cancer Res. 59, 4383–4391.
Ye, Z.C., Rothstein, J.D., Sontheimer, H., 1999. J. Neurosci. 19, 10767–10777.
Zhang, H., Lin, S.C., Nicolelis, M.A.L., 2009. J. Neurosci. Methods 179, 191–200. https://doi.org/10.1016/j.jneumeth.2009.01.023.
Zhou, Y., Danbolt, N.C., 2014. J. Neural Transm. 121, 799–817. https://doi.org/10.1007/s00702-014-1180-8.